$SICNet_{season}$ V1.0: a transformer-based deep learning model for seasonal Arctic sea ice prediction by incorporating sea ice thickness data

Yibin Ren[1], Xiaofeng Li[1], Yunhe Wang[1]

[1]Key Laboratory of Ocean Observation and Forecasting, Key Laboratory of Ocean Circulation and Waves, Institute of Oceanology, Chinese Academy of Sciences, Qingdao, China

Correspondence to: Xiaofeng Li (lixf@qdio.ac.cn)

Abstract. The Arctic sea ice suffers dramatic retreating in summer and fall, which has far-reaching consequences on the global climate and commercial activities. Accurate seasonal sea ice predictions significantly infer climate change and planning commercial activities. However, seasonally predicting the summer sea ice encounters a significant obstacle known as the spring predictability barrier (SPB): predictions made later than the date of melt onset (roughly May) demonstrate good skill in predicting summer sea ice, while predictions made on or earlier than May exhibit considerably lower skill. This study develops a transformer-based deep-learning model, $SICNet_{season}$ (V1.0), to predict the Arctic sea ice concentration on a seasonal scale. Including spring sea ice thickness (SIT) data in the model significantly improves the prediction skill at the SPB point. A 20-year (2000-2019) testing demonstrates that the detrended anomaly correlation coefficient (ACC) of Sep. sea ice extent (sea ice concentration > 15%) predicted by our model at May/Apr. is improved by 7.7%/10.61% over the ACC predicted by the state-of-the-art dynamic model SEAS5 from the European Centre for Medium-Range Weather Forecasts (ECMWF). Compared with the anomaly persistence benchmark, the mentioned improvement is 41.02%/36.33%. Our deep learning model significantly reduces prediction errors of Sep.'s sea ice concentration on seasonal scales compared to SEAS5 and Persistence. The spring SIT data is key in optimizing the predictions around the SPB, contributing to a more than 20% ACC enhancement in Sep.'s SIE at four to five months lead predictions. Our model achieves good generalization in predicting the Sep. SIE of 2020-2023.

1 Introduction

Arctic sea ice plays a significant role in the global climate because it modulates the thermal and dynamic exchanges between the ocean and the atmosphere(Ding et al., 2017; Kapsch et al., 2013; Liu et al., 2021a; Olonscheck et al., 2019). In recent decades, global warming has resulted in a dramatic retreat in Arctic sea ice during the summer and fall (Cao et al., 2017; Shu et al., 2022). This decline triggers a system-positive feedback mechanism that causes the Arctic's surface air temperature to increase 2-4 times faster than the global mean state, known as the Arctic amplification (AA) (England et al., 2021; Pithan and Mauritsen, 2014; Screen et al., 2013; Screen and Simmonds, 2010). AA accelerates sea ice decline, strengthening positive

feedback (Jenkins and Dai, 2021; Kumar et al., 2010). If the situation is unchanged, climate models project that the Arctic will become ice-free during summer by the 2050s (Jahn et al., 2024; Kim et al., 2023). The dramatic Arctic sea ice loss has consequences for global climate (Francis and Vavrus, 2012) and commercial activities (Min et al., 2022). For example, it may weaken the stratospheric polar vortex in the winter, increasing extreme cold events in the Northern Hemisphere (Blackport et al., 2019; Cohen et al., 2014). Furthermore, the lower sea ice area during summer extends the navigability of the Arctic Passage to seasonal scales (Cao et al., 2022).

Sea ice predictions are helpful for better understanding global climate change and support human activities in the Arctic (Lindsay et al., 2008; Merryfield et al., 2013). Therefore, sea ice prediction, commonly represented by parameters such as sea ice concentration (SIC) or sea ice extent (SIE, defined as the sum of grid cell area where SIC>15%), has always attracted substantial efforts (Guemas et al., 2016; Stroeve and Notz, 2015). Various prediction systems are proposed, such as numerical (Chevallier et al., 2013; Liang et al., 2020; Mu et al., 2020; Wang et al., 2013; Yang et al., 2019; Zhang et al., 2008, 2022), statistical (Gregory et al., 2020; Wang et al., 2016, 2022; Yuan et al., 2016), and deep learning models (Jun Kim et al., 2020; Ren et al., 2022; Ren and Li, 2023). However, accurate sea ice prediction for Arctic summer remains challenging, particularly at seasonal or even longer scales (Zampieri et al., 2018; Blanchard-Wrigglesworth et al., 2015, 2023). One of the biggest challenges is the spring predictability barrier (SPB): predictions for summer sea ice made before or at the timing of melt onset show significantly lower skill than predictions made after the timing of melt onset (Bonan et al., 2019; Bushuk et al., 2020; Day et al., 2014; Zeng et al., 2023). Studies show that SPB is evident in nearly all the fully coupled global climate models (GCMs) in Phase 5 of the Coupled Model Intercomparison Project (CMIP5), a crucial initiative providing climate projections to support essential climate research worldwide (Blanchard-Wrigglesworth et al., 2011; Tietsche et al., 2014). So, optimizing the predictions around the SPB is an urgent task for accurate summer sea ice predictions.

Experiments based on ensemble simulations reveal that the predictability of summer SIE is limited before spring due to the ice motion and growth in winter (Bushuk et al., 2020). However, the predictability increases rapidly after the melting processes in the spring (Bushuk et al., 2020). The satellite observations show that the spring sea ice thickness (SIT) correlates more with the summer SIE than the spring SIE (Landy et al., 2022). These findings indicate that the spring SIT may be a key factor in optimizing the predictions around the SPB (Bushuk et al., 2020). Recently, researchers have assimilated the CryoSat-2 observed SIT data, the first summer SIT observations, into the Geophysical Fluid Dynamics Laboratory (GFDL) ocean–sea ice model and found that the prediction skill of Sep.'s SIC is improved significantly when the model is initialized with SIT anomaly in Jul. and Aug. (Zhang et al., 2023). This study further proves that the summer SIT data contributes to Sep's sea ice prediction. However, as the SPB flag is May for most studies, whether the predictions around the SPB could be optimized by including SIT data remains largely unknown.

Currently, numerical models are widely used in operationally sea ice predicting, but they are inflexible and have been limited by the SPB (Msadek et al., 2014; Sigmond et al., 2013). Statistical models are good at long-term prediction but cannot model complex nonlinear relationships and face SPB challenges. Deep learning models are more flexible than numerical models and more potent than traditional statistical ones, and they have been successfully used in Earth prediction problems (Li et al., 2021;

Reichstein et al., 2019). Researchers have successfully developed deep-learning models to predict polar sea ice state from synoptic to sub-seasonal scales (Andersson et al., 2021; Dong et al., 2024; Li et al., 2024; Mu et al., 2023; Palerme et al., 2024; Ren et al., 2022; Ren and Li, 2023; Song et al., 2024; Wu et al., 2022; Yang et al., 2024.; Zhu et al., 2023), bringing the new potential to solve the SPB problem to improve the seasonal prediction skill from a data-driven perspective.

This work develops a seasonal sea ice prediction model named $SICNet_{season}$ (V1.0) to optimize the predictions around the SPB. $SICNet_{season}$ is a transformer-based deep learning model with a physically constrained loss function based on SIC morphology. It takes historical SIC and SIT data as predictors and predicts the SIC of the following six months. The SIC data is the satellite-observed data from the National Snow and Ice Data Center (NSIDC) (Cavalieri et al., 1996). The $SICNet_{season}$ model is trained on data from 1979-2019 and tested with data from 2000-2019 by a leave-one-year-out strategy. Data from the recent four years, 2020-2023, is employed to verify the model's generalization. Experiments demonstrate that our model significantly optimizes the SPB with a higher detrend correlation coefficient (ACC) compared with anomaly persistence (Persistence) and the state-of-the-art dynamic model, SEAS5, from the European Centre for Medium-Range Weather Forecasts (ECMWF) (Johnson et al., 2019). Our model significantly reduces the errors in September. SIC/SIE in four to five months lead predictions compared to the two compared models. The spring SIT data is key in optimizing the predictions around the SPB. Our model generalized well in predicting the Sep. SIE of 2020-2023. Finally, we compare our $SICNet_{season}$ model with an IceNet-inspired U-Net model (Andersson et al., 2021). IceNet is a probability prediction model for Arctic SIE based on convolutional neural network (CNN) units and the U-Net architecture. It achieved state-of-the-art performance in predicting the probability of SIE for six months (Andersson et al., 2021). Therefore, we construct an IceNet-inspired U-Net model as a comparison model.

2 Data

1.1 Sea ice concentration data

The SIC data of 1979-2023 are experiment data. The SIC is the satellite-observed data obtained from the NSIDC. It is a daily observation derived from the Nimbus-7 Scanning Multichannel Microwave Radiometer (SMMR) and the Defense Meteorological Satellite Program (DMSP) Special Sensor Microwave Imager (SSM/I and SSMIS) (DiGirolamo et al., 2022). The projection of the SIC data is the north-polar stereographic with a 25 km spatial resolution.

1.2 Sea ice thickness data

The SIT data is the reanalysis SIT from the Pan-Arctic Ice Ocean Modeling and Assimilation System (PIOMAS). PIOMAS is a numerical model with sea ice and ocean components, and it assimilates SIC and sea surface temperature (Zhang and Rothrock, 2003). PIOMAS SIT agrees well with in situ, airborne, and satellite measurements (Schweiger et al., 2011). It is daily data with an 18 km spatial resolution. Although the PIOMAS generally overestimates thin ice and underestimates thick ice regions, it is widely adopted by Arctic studies (Collow et al., 2015; Kwok et al., 2020; Nakanowatari et al., 2022). The SIC and PIOMAS SIT data are converted to a Northern Polar Stereographic Grid with 80 km resolution. The temporal resolution

95 is one month.

3 Method

3.1 Framework of SICNet$_{season}$

The SICNet$_{season}$ model is derived from a transformed-based U-Net deep learning model, SwinUNet (Cao Hu and Wang, 2023)(Cao Hu and Wang, 2023). It accepts a three-dimensional sea ice data sequence and predicts a three-dimensional SIC
100 sequence of the future, Fig. 1. The inputs to the model are monthly mean fields. The predicted target is the SIC of the next six months. For example, if we make predictions in May, the six months' predictions will cover the months from Jun. to Nov.

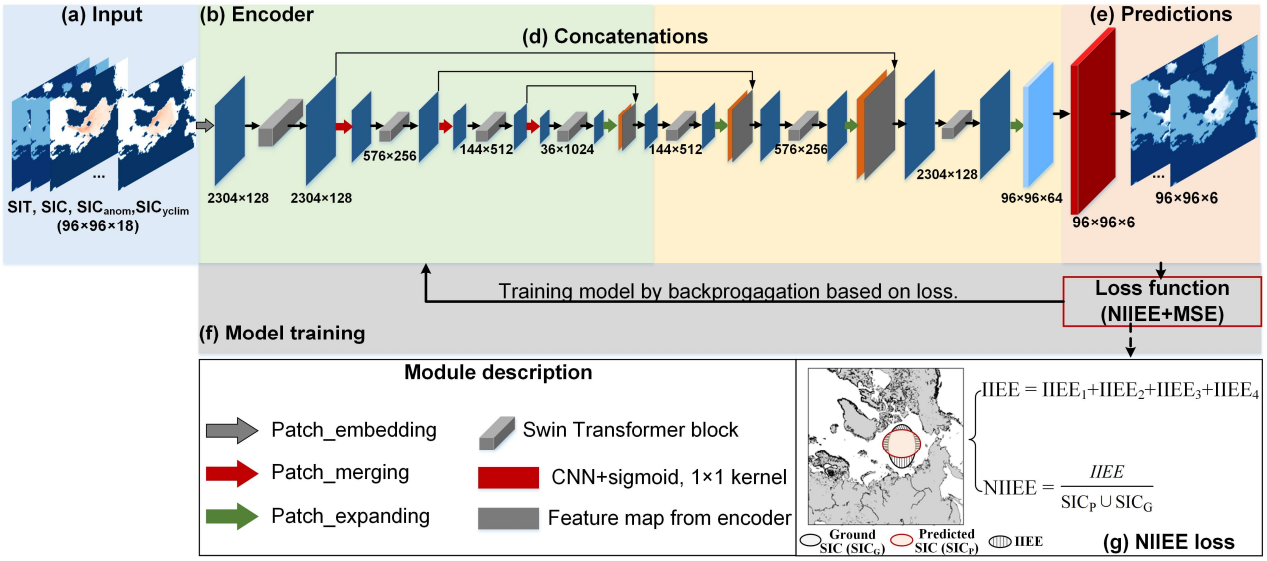

Figure 1. Framework of model SICNet$_{season}$. (a) Input consists of SIT of the last three months, SIC of the last six months, SIC anomaly of the last three months, and SIC climatology of six target months, 96×96×18. (b) The encoder comprises four swin-transformer
105 **blocks and three patch-merging operators. (c) The decoder contains three swin-transformer blocks and four patch-expanding operators. (d) Concatenations connect the feature maps from the encoder and the decoder module. (e) A CNN layer with sigmoid activation transforms the feature map to the predicted SIC of six-month leads. (f) Model training procedure. The loss function combines the normalized integrated ice-edge error (NIIEE) and the mean square error (MSE).**

110 The input for SICNet$_{season}$ is a 96×96×18 SIC and SIT sequence, composed of SIT of the last three months, SIC of the last six months, SIC anomaly of the last three months, and SIC climatology of the six target months (Fig. 1a). We determine the length of input factors by combining domain knowledge and manual tuning experiments. The primary domain knowledge we considered is the spring-fall reemergence mechanism. It occurs between pairs of months where the ice edge is in the same position, such as in May and December (Blanchard-Wrigglesworth et al., 2011; Day et al., 2014). The spring sea ice anomaly
115 is positively correlated with fall sea ice anomalies, and there is also a weaker reemergence between fall sea ice anomalies and anomalies the following spring (Bushuk et al., 2015). Therefore, we set the initial input length of the SIC/SIT/SIC anomaly as

six months. We change the input length manually (from six to one in step one) to fine-tune the deep learning model to find the best-matched length for each factor. The SIC climatology of the target months provides an essential mean state of the prediction SIC. It represents the monthly cycle signal that IceNet has considered (Andersson et al., 2021).

The input is fed into the encoder to capture spatiotemporal correlations among SIC/SIT data sequences at different levels to form multi-scale correlation maps. The encoder comprises four swin-transformer (Liu et al., 2021b) blocks and three patch merging operators (Fig. 1b). A swin-transformer block is a transformer unit integrated with shifted windows (Liu et al., 2021b). A transformer operator captures global dependencies through an attention mechanism. The shifted windows help the transformer operator capture local dependencies like the convolution operator. Therefore, local and global spatiotemporal dependencies among sea ice sequences can be captured. The patch merging operator downscales the captured feature maps like the pooling layer in CNN models. The decoder upscales the feature maps through the patch expanding operator and swin-transformer blocks (Fig. 1c). The extracted correlation maps of the encoder and decoder are stacked to form fused spatiotemporal maps (Fig. 1d). A CNN layer transforms the decoded feature maps to the same shape as the target SIC sequence. Here, it is a 96×96×6 array (Fig. 1e). As the range of SIC is 0-1, we employ the sigmoid function to activate the last feature map to transform the predicted values to 0-1.

During the training procedure, the loss is calculated between the predicted and ground values. Then, the model's parameters are trained by minimizing the loss value literately. We will explain the loss function in the following section.

3.2 Integrated ice-edge-constrained loss function

For a deep-learning model, the loss function is crucial during the training procedure as it guides the optimization of the model's parameters. Here, the loss is the difference between the predicted values and the ground ones from NSIDC. Generally, the mean square error (MSE) is a fundamental loss function for prediction tasks. The MSE measures the mean state for all predicted values and cannot reflect the spatial differences between 2-dimensional SIC patterns. To address the issue, we proposed a normalized integrated ice-edge error (NIIEE) loss function that considers the spatial distribution of SIC to constrain the model's optimization (Fig. 1g).

The NIIEE loss is based on the integrated ice-edge error (IIEE), a professional metric for sea ice predictions. The IIEE represents the error regions the prediction model overestimated and underestimated (Goessling et al., 2016). It measures the spatial similarity between two 2-dimension SIC patterns. Initially, the IIEE binaries the SIC by 15% to describe the SIE. For the SIC prediction here, we do not perform binarization. Let P_{SIC}/G_{SIC} represent the predicted/ground SIC; the IIEE is calculated by Eq. (1). We normalize IIEE to the range of 0-1 to form the NIIEE loss by Eq. (2). If the NIIEE loss is 0, the predicted SIC and the ground SIC will match in spatial and numerical. The fundamental MSE loss has been demonstrated to be adequate for prediction tasks. If the number of all predicted values is N, the MSE is calculated by Eq. (3). We combine the NIIEE with MSE as the loss function of the $\text{SICNet}_{\text{season}}$. A constant scale factor, 0.01, is multiplied by NIIEE to balance its range with that of MSE, Eq. (4).

$$IIEE = (P_{SIC} \cup G_{SIC}) - (P_{SIC} \cap G_{SIC}) \quad (1)$$

$$NIIEE = \frac{IIEE}{P_{SIC} \cup G_{SIC}} = 1 - \frac{P_{SIC} \cap G_{SIC}}{P_{SIC} \cup G_{SIC}} \quad (2)$$

$$MSE = \frac{\sum (P_{SIC} - G_{SIC})^2}{N} \quad (3)$$

$$Loss = 0.01 \times NIIEE + MSE \quad (4)$$

4 Experiments

4.1 Model training

The model is trained on a computer station with an NVIDIA Tesla V100 32-GB card. The training and test samples are constructed by step-by-step sliding. The testing period is 2000-2019. The leave-one-year-out strategy is adopted to train/evaluate our $SICNet_{season}$ model. For example, if the testing year is 2000, the training set is from 1979-1999 and 2001-2019. The leave-one-year-out strategy is widely adopted by statistical models to maximize the sample volume while obtaining a multi-year evaluation (Wang et al., 2022; Yuan et al., 2016). The validation set is split 20% from the training set. We set the batch size as eight and the initial learning rate as 0.0001. We employ the early stopping strategy to break the training procedure when the validation loss does not decrease. The model is trained three times to eliminate random errors. The testing set is run on three trained models, and the mean values are adopted as the final predictions. Data from the recent four years, 2020-2023, is employed to verify the model's generalization. Data from these four years did not participate in the training stage. They are fed into the trained models obtained by the leave-one-year-out strategy to get the predictions. The predictions are the mean values of the 20 trained models.

4.2 Evaluation metrics

The mean absolute error (MAE), Binary Accuracy (BACC), and detrend ACC are evaluation metrics. The MAE is for SIC, and the other two metrics are for SIE. To accurately calculate the metrics, we use the maximum observed monthly SIE since 1979 to mask the predictions. Assuming the predicted/truth value of the i_{th} grid is p_i/g_i, the number of validation grids is N. The MAE values are calculated by (5). The BACC of time t is obtained by using one to subtract the ratio of IIEE to the area of the activated grid cell region (the maximum observed SIE during 1979-2019) of t by equation (6). The detrend ACC of SIE is the anomaly correlation coefficient of two detrend SIE series. Each SIE series has 20 elements, from 2000 to 2019.

$$MAE = \frac{\sum_1^N |p_i - g_i|}{N} \quad (5)$$

$$BACC = \left(1 - \frac{IIEE}{\text{area of the activated grid cell region}}\right) \times 100\% \quad (6)$$

4.3 Model skill in seasonal predictions

We compare the $SICNet_{season}$ with the Persistence and the SEAS5 to validate our model's ability to optimize the predictions around the SPB. The Persistence is the anomaly persistence model. It assumes the anomaly constant in time and estimates the target SIC values by adding the current anomaly to the climate mean state at the target time, widely adopted as a benchmark for sea ice prediction (Wang et al., 2016). The SEAS5 is a new seasonal forecast system from the ECMWF that shows excellent sea ice prediction skills (Johnson et al., 2019). A BACC value of 100% indicates that the predicted SIE matches the observed SIE 100% spatially. The metrics are calculated for 20 testing years, 2000-2019, in a leave-one-year-out training/testing strategy. As the SPB occurred in the target summer month, we focus on the four summer months, June to September.

Fig. 2 shows the detrended ACC and BACC of target months, Jun.-Sep., on six lead months' predictions. As shown in Figs. 2(a) and (b), the predictions of Persistence and SEAS5 show an apparent SPB: the detrended ACC drops sharply when the predictions are made earlier than May, with a maximum ACC gap between two adjacent lead months marked by black lines. Taking September for example, the detrend ACC is 56.39% for Persistence when the prediction is made in Jun. (three months lead). Then, it decreases to 26.59% in May's prediction (four months lead), Fig. 2(a). For SEAS5, the ACC of Jun.'s prediction is 83.94%, then drops to 59.91% at May's prediction, forming a 24.03% ACC gap, Fig. 2(b). Although the $SICNet_{season}$'s prediction also shows an SPB feature, the black line in Fig.2 (c), the ACC at May's prediction is improved to 67.61%, and the ACC gap is reduced to 15.6%. Further, the ACC difference is calculated between $SICNet_{season}$ and Persistence/SEAS5. Compared with Persistence, $SICNet_{season}$ improves the ACC in most predictions, Fig. 2d. The ACC improvements along the SPB flag are more than 30% on average (the lead months right to the black line in Fig. 2d). Compared with the SEAS5, $SICNet_{season}$ also improves the prediction skill of the SPB. When the target months are Jun. and Jul., $SICNet_{season}$ shows a much higher prediction skill than SEAS5 in four to six months lead predictions, Fig. 2e. For the target month Sep., the $SICNet_{season}$ improves the ACC by 7.70%/10.61% than SEAS5 when prediction is made in May/Apr. (four/five months lead in Fig. 2e). For the target month Aug./Sep., the $SICNet_{season}$ shows lower ACCs than the SEAS5 when prediction is made on or before Mar. (five/six months lead for Aug./Sep.). However, for the predictions made adjacent to the SPB flag line, the $SICNet_{season}$ achieves larger ACCs than the SEAS5 (values right to the black line in Fig. 2e). Therefore, the $SICNet_{season}$ optimizes the SPBs significantly compared to the well-known numerical model.

The BACC of SEAS5 also shows a similar SPB characteristic to the ACC. A sharp BACC drop occurred when the prediction was made on and before May, the black line in Fig. 2(g). The maximum BACC gaps of Persistence and $SICNet_{season}$ occurred in the second lead month. However, the maximum BACC gap of $SICNet_{season}$ is about 2%, much lower than the 10% gap of Persistence and SEAS5. Compared with the Persistence and SEAS5, the $SICNet_{season}$ improves the BACC by more than 10% in predicting SIE of Aug. and Sep. three to six months lead, Figs. 2(i) and (j).

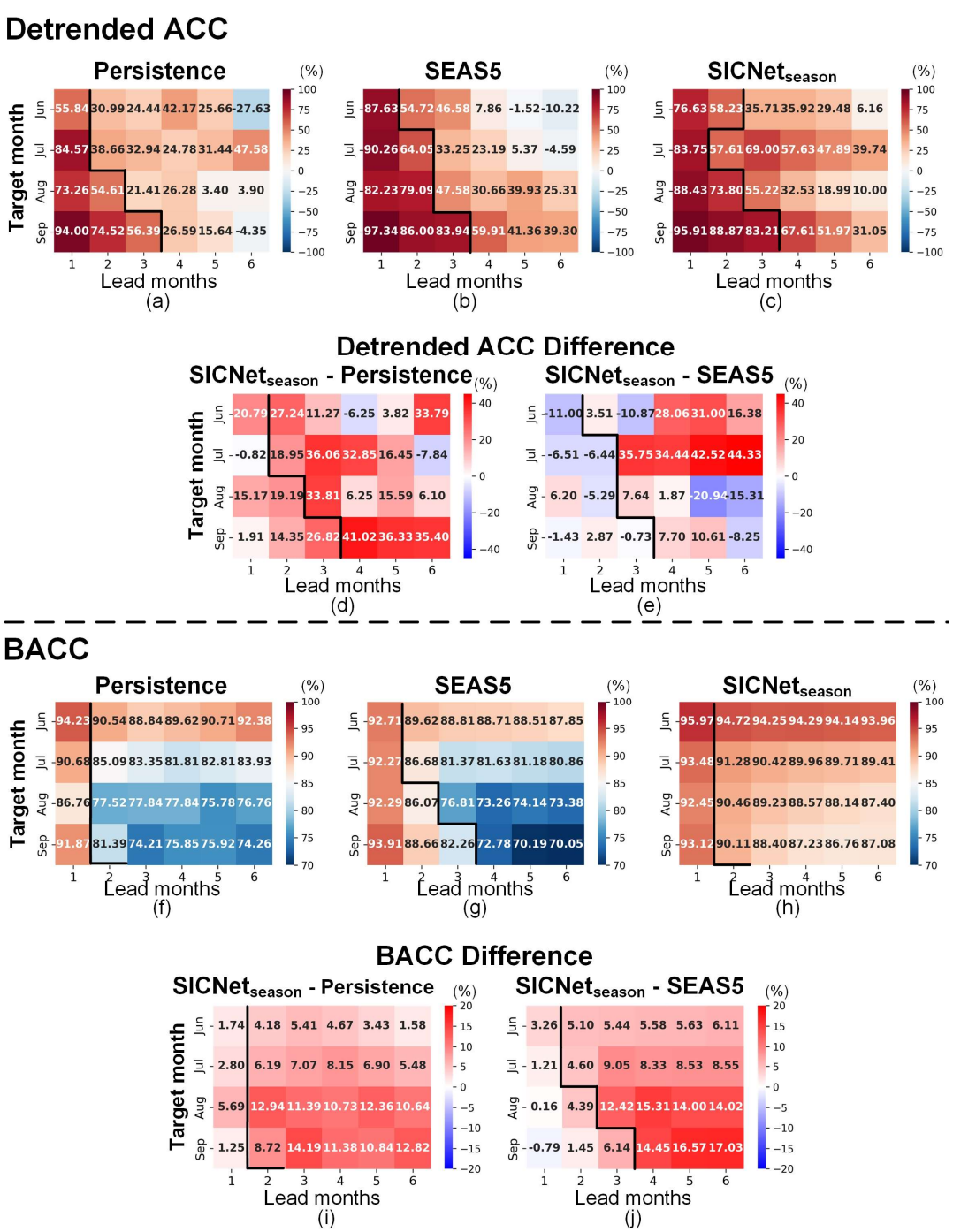

Figure 2. Detrend ACC of SIE, BACC of SIE, and their differences of Persistence, SEAS5, and SICNet$_{season}$ from Jun. to Sep., averaged by 2000-2019. (a)-(c) Detrend ACC of three models. Two detrend SIE series (predicted and observed) calculate each value. (d)-(e) Detrend ACC differences between SICNet$_{season}$ and Persistence/SEAS5. (f)-(h) BACC of three models. Each BACC is a mean value during 20 testing years. (i)-(j) BACC differences of SICNet$_{season}$ and Persistence/SEAS5. The black line indicates the SPB: a maximum decrease between two adjacent lead months. The red signifies a high/improvement in ACC/BACC, and the blue signifies a decrease.

4.4 Performance in predicting SIC of Sep.

As September's sea ice draws wider attention than other months, we calculate the MAE of SIC of Sep. predicted by three models. Fig. 3 shows the spatial MAE of Persistence, SEAS5, and $SICNet_{season}$ on six lead months. The MAE in the three models is not much different for the first two lead months. When the lead month is one, the MAE of SEAS5 is slightly better than that of Persistence and $SICNet_{season}$, indicating that the SEAS5 model performs well in monthly predicting. This result may be due to the good atmospheric initialization in SEAS5, which beat many machine learning and dynamical models in sub-seasonal scale SIC prediction (Bushuk et al., 2024). However, when the lead month is longer than three, the SEAS5's MAEs are much more than 45% in the Pacific sector, mainly containing the Beaufort Sea, the Chukchi Sea, the East Siberian Sea, and the Laptev Sea, Figs. 3(j)-(l). The $SICNet_{season}$ reduces the MAEs to 20-30% for most regions in the Pacific Arctic, Figs. 3(q)-(r). Compared with Persistence, $SICNet_{season}$ also reduces MAEs by 5-10% in the mentioned four local seas, Figs. 3(d)-(f). Therefore, the $SICNet_{season}$ significantly reduces the SIC errors of Sep. in seasonal scale predictions (three to six months lead).

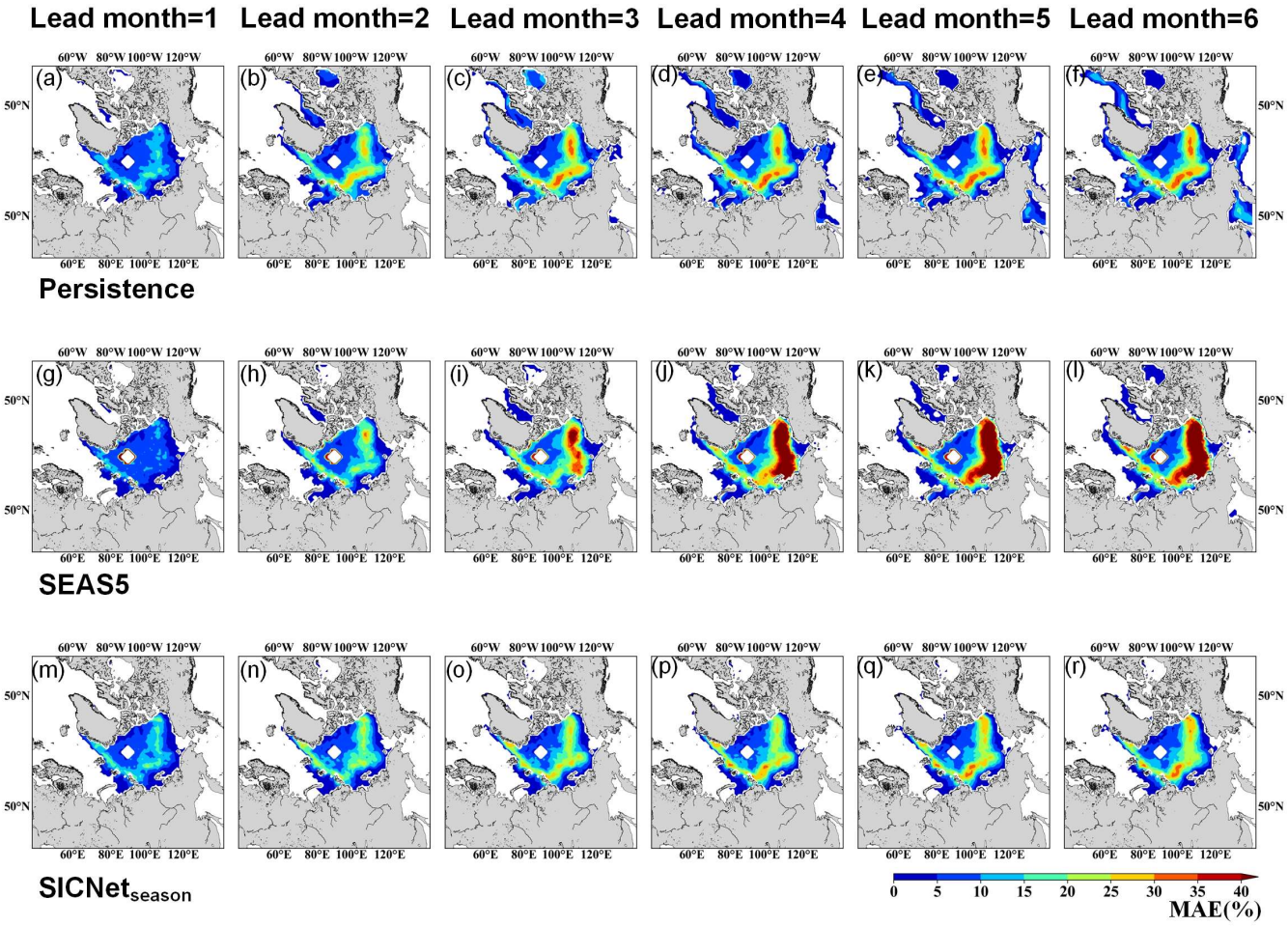

Figure 3. The MAEs of September's predictions are based on three compared models: each value is averaged by 20 testing years. (a)-(g) MAEs of Persistence. (h)-(m) MAEs of SEAS5. (n)-(s) MAEs of $SICNet_{season}$.

4.5 SIT's contributions to seasonal predictions

We further conduct a comparison experiment to validate the role of SIT data in seasonal predictions based on $SICNet_{season}$. The model without SIT as an input is named $SICNet_{season\_nosit}$. The other settings for $SICNet_{season\_nosit}$ are the same as those for $SICNet_{season}$. The detrended ACC and BACC are shown in Fig. 4.

Without the SIT data as input, the model's prediction skill drops apparently in three to six months lead predictions, Fig. 4(a). For the target month Sep., the detrend ACC is 76.41% when the prediction is made in Jun. (three months' lead). Then, the ACC drops to 26.43% at May's prediction (four months' lead). By including SIT data as input, the ACC of May's prediction is improved by 41.18% in model $SICNet_{season}$, Fig. 4(c). For the target month of August, the ACC improvement at May's prediction (three months' lead) by including SIT data is 42.44%. Therefore, the SIT data is important to improve the model's prediction skill on SPB.

For target months Aug. and Sep., the BACCs of $SICNet_{season\_nosit}$ show an apparent drop in three to six months lead predictions. By including SIT data as the model's input, the BACC improvement is 0.95%/2.02% for the target month, Aug./Sep. at May's predictions, Fig. 4(f). Then, we calculate the MAE of the target month Sep., Fig. 5. The MAEs of the first two lead months are similar for the two models. When the lead month is larger than three, the MAEs of $SICNet_{season\_nosit}$ in the Beaufort Sea, the East Siberian Sea, and the Laptev Sea are 30-45%, with red circles in Figs. 5(d)-(f). By including SIT data, the MAEs in the three mentioned regions are reduced to 20-35% by SICNetseason, as shown in the red circles in Figs. 5(j)-(l). Therefore, including SIT data reduces the errors of Sep.'s SIC by more than 10% in seasonal scale predictions.

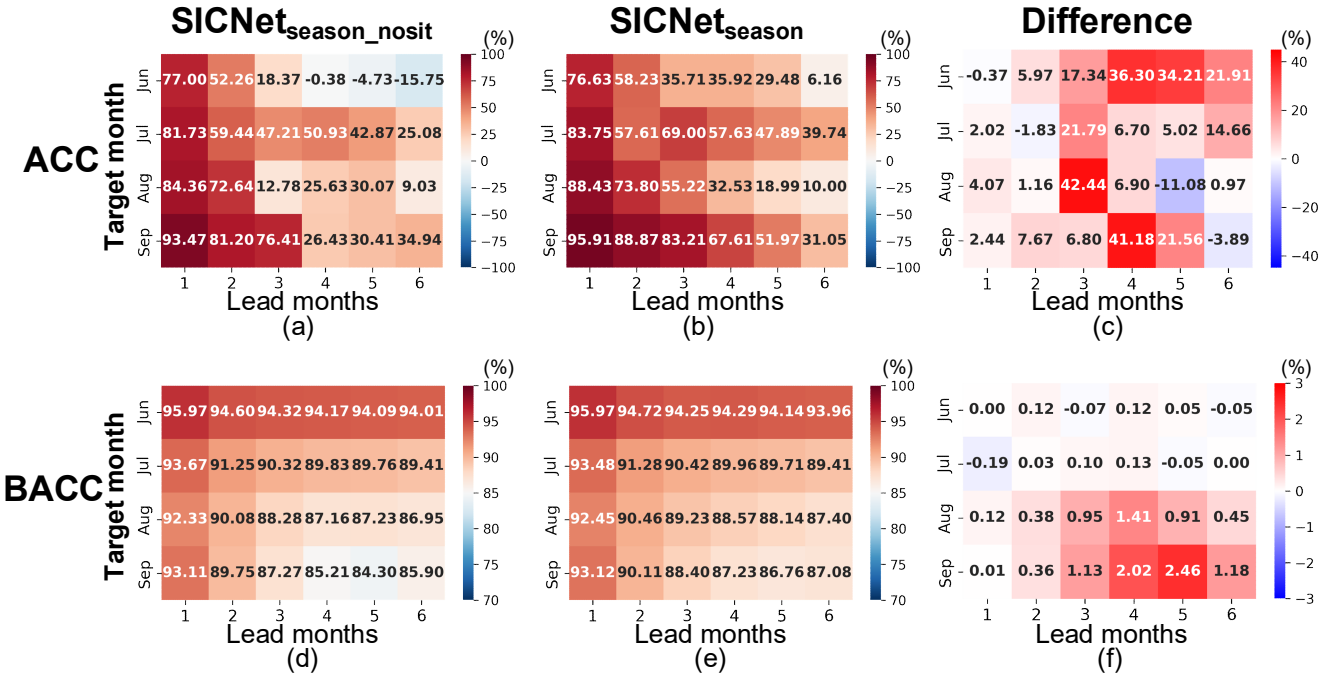

Figure 4. Detrended ACC of SICNet$_{season_nosit}$ (a) and SICNet$_{season}$ (b). (c) ACC difference obtained by SICNet$_{season}$ minus SICNet$_{season_nosit}$. BACC of SICNet$_{season_nosit}$ (d) and SICNet$_{season}$ (e). (f) BACC difference like (c). The red signifies a high/improvement in ACC/BACC, and the blue signifies a decrease.

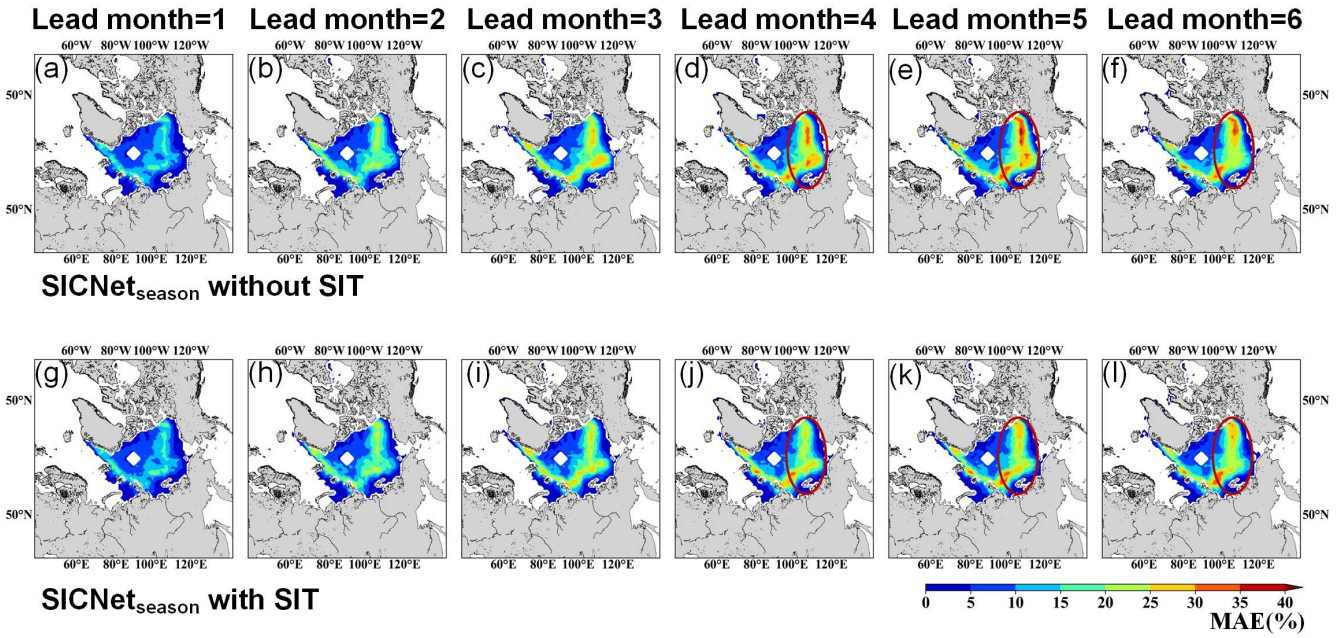

Figure 5. The MAEs of Sep.'s SIC predicted by SICNet$_{season}$ and SICNet$_{season_nosit}$. Each value is averaged by 20 testing years. (a)-(g) MAE of SICNet$_{season_nosit}$. (h)-(m) MAE of SICNet$_{season}$. The red cycles marked the regions where the MAE is reduced typically by including SIT data.

4.6 Generalization in predicting the SIEs of 2020-2023

To verify our model's generalization in predicting the SIEs of recent years, we employed the twenty trained models to predict the SIE of the recent four years, 2020-2023. The twenty models are trained for 2000-2019, as mentioned in the earlier sections. The data from 2020-2023 is "blind" for the models. The mean values of the twenty models' predictions are the final predictions. As the temporal span of four years is too short for calculating ACC, we use the BACC as the metric (Fig. 6). Compared with Persistence and SEAS5, the $SICNet_{season}$ achieves higher BACCs in predicting SIEs of Aug. and Sep. For the target month Sep., the BACC of $SICNet_{seaon}$ is 10% higher than those of the other two models in three to six months lead predictions.

We draw the observed and predicted Sep.'s SIEs of 2020, 2022, and 2023 in Fig. 7. The Sep.'s SIE in 2020/2023 (4.0/4.37 $milkm^2$) is the second/sixth lowest record in the Arctic since 1979. The SIE in 2022 Sep. (4.90 $milkm^2$) has been large since 2015. We focus on the seasonal scale predictions with four to six lead months. Our $SICNet_{season}$ model shows obvious advantages over the SEAS5 and Persistence. For predictions made on or before May, lead months of four to six, the BACCs of $SICNet_{season}$ are much higher than those of Persistence and SEAS5, Fig. 7. At May's prediction, our model achieved a BACC of 82.25%/90.39%/82.08% in 2020/2022/2023, more than 10% higher over the Persistence and SEAS5, Fig. 7(a)/(d)/(g). Therefore, the $SICNet_{season}$ model achieves good generalization in predicting the SIEs of 2020-2023.

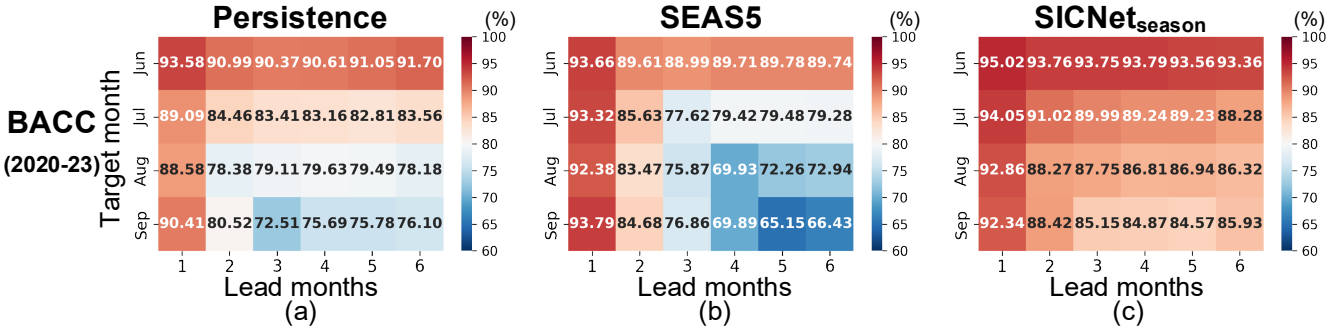

Figure 6. BACC of 2020-2023. (a) Persistence, (b) SEAS5, and (c) $SICNet_{season}$. Each value is a mean value of the four testing years. The horizontal axis represents the six lead months, and the vertical axis represents the target months, Jun. to Sep. The red signifies a high/improvement in ACC/BACC, and the blue signifies a decrease.

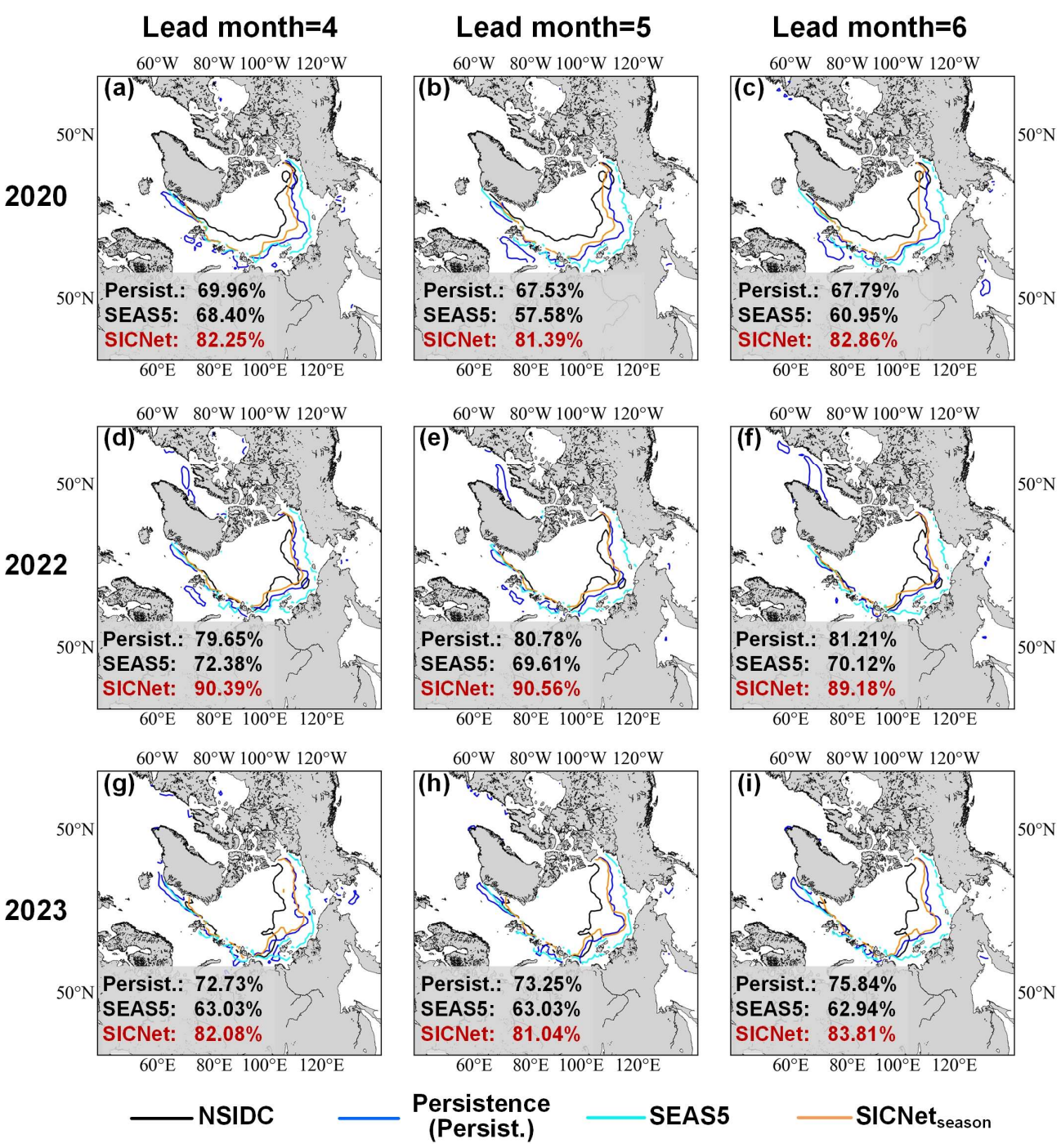

Figure 7. Predicted Sep. SIEs and their BACCs of 2020/2022/2023 in four to six months lead by Persistence, SEAS5, and SICNet$_{season}$. (a)-(c) 2020, (d)-(f) 2022, and (g)-(i) 2023.

4.7 Comparison with the representative deep learning model

We compare the SICNet$_{season}$ against the representative deep learning sea ice prediction model, the U-Net (IceNet-inspired) model. The IceNet is a seasonal sea ice prediction model that performs state-of-the-art SIE probability prediction (Andersson et al., 2021). It is a CNN-based U-Net model for classification tasks, and it outputs the probability of three classes: open water (SIC≤15%), marginal ice (15% < SIC < 80%), and full ice (SIC≥80%). Differently, our SICNet$_{season}$ outputs the 0-100% range SIC values. The IceNet's inputs consist of 50 monthly mean variables, including SIC, 11 climate variables, statistical SIC forecasts, and metadata. The original IceNet model has some unique designs in inputs and training strategy. As we focus on the differences in model structures, we construct a U-Net (IceNet-inspired) model for comparison.

We set the inputs (including SIT data) of the U-Net (IceNet-inspired) to the same ones as SICNet$_{season}$. The loss function is also set as the NIIEE+MSE. We set the output layer of U-Net (IceNet-inspired) as a sigmoid activation function to output continuous values of 0-100%. We also change the number of CNN filters to make the number of training parameters in U-Net (IceNet-inspired) equal to that in SICNet$_{season}$, about 140 million. The training and testing settings of U-Net (IceNet-inspired) are the same as those of SICNet$_{season}$. The U-Net (IceNet-inspired) is trained using the same leave-one-year-out strategy as the SICNet$_{season}$. For example, if the testing year is 2019, the training set is data from 1979-2018, and the testing data is 2019. Then, the testing data moves to 2018; the remaining data (1979-2017, 2019) is the training set. For each training/testing pair, the model is trained three times to eliminate randomness, and the final prediction for testing data is the mean value of the three models.

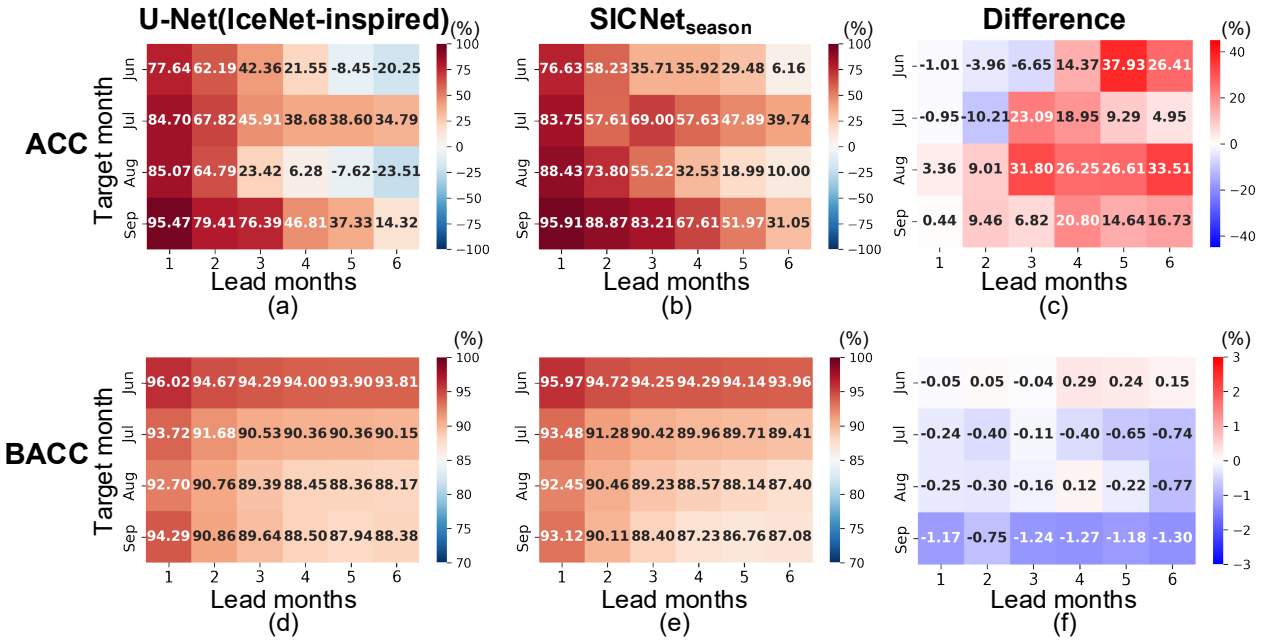

Figure 8. Detrended ACC of U-Net (IceNet-inspired) (a) and SICNet$_{season}$ (b). (c) ACC difference obtained by SICNet$_{season}$ minus U-Net (IceNet-inspired). BACC of U-Net (IceNet-inspired) (d) and SICNet$_{season}$ (e). (f) BACC difference like (c). The red signifies a high/improvement in ACC/BACC, and the blue signifies a decrease.

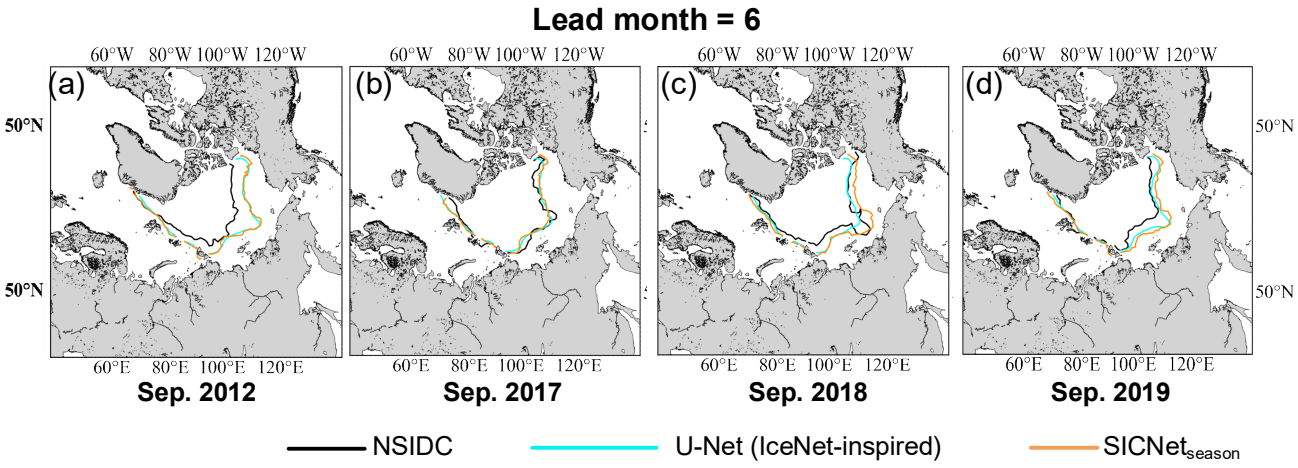

Figure 9. The predicted Sep. SIEs of U-Net (IceNet-inspired) and SICNet$_{season}$ in six months' lead: (a) 2012, (b) 2017, (c) 2018, and (d) 2019.

Fig. 8 shows the detrend ACC, BACC, and the differences between the two models. Compared with the U-Net (IceNet-inspired) model, our SICNet$_{season}$ model significantly improves the ACC at most predictions, Fig. 8(c). For the target month, Aug./Sep., the SPB feature is obvious in the U-Net (IceNet-inspired): the maximum ACC gap is about 40%/30% at predictions made in May and Jun., Fig. 8(a). Our SICNet$_{season}$ model optimizes the ACC gap with an improvement of 31.8%/20.8% at May's predictions, Fig. 8(c). The ACC improvements are also larger than 15% for predictions made before May. Therefore, compared with the state-of-the-art deep learning model U-Net (IceNet-inspired), our model achieves more skillful seasonal predictions by optimizing the predictions around the SPB.

Unlike the ACC values, the BACC values of U-Net (IceNet-inspired) are more significant than those of SICNet$_{season}$ on most predictions, Fig. 8(f). This result implies that U-Net (IceNet-inspired) depends more on SIE trends than SICNet$_{season}$. This difference can be attributed to the distinct fundamental units employed by the two models. The U-Net (IceNet-inspired) is a CNN-based model, and the weight-sharing mechanism of convolutional kernels forces the model to capture the most "common" local dependencies in spatial. Though representative, these "common" local dependencies tend to yield smoother model outputs. The SICNet$_{season}$ is a transformer-based model. The attention mechanism of the transformer can capture global dependencies without weight-sharing. As a result, "personalized" global dependencies are extracted, and the output is not smooth like the output of a CNN-based model. The "common" local dependencies have more apparent trend features than the "personalized" global dependencies. Fig. 9 shows the Sep.'s SIEs predicted by U-Net (IceNet-inspired) and SICNet$_{season}$ in the sixth-month lead. The SIEs of U-Net (IceNet-inspired) are smoother than those of SICNet$_{season}$. For 2012 and 2017, the SIEs' locations of the two models are very similar. For the other two years, the SIEs of U-Net (IceNet-inspired) match the observed SIEs better than those of SICNet$_{season}$. However, the SIEs of U-Net (IceNet-inspired) are over-smoothed and fail to characterize some abnormal characteristics, such as the SIE in Sep. 2018, Fig. 9(c).

Therefore, our transformer-based $SICNet_{season}$ is more skillful than the representative CNN-based model U-Net (IceNet-inspired) in optimizing the predictions around the SPB. The $SICNet_{season}$ exhibits a lower dependency on SIE trends and lower smooth results than the CNN-based model.

5 Conclusion

This study develops a deep-learning model, $SICNet_{season}$, to predict the Arctic SIC on a seasonal scale. The model is derived from a SwinUNet architecture. It inputs the historical SIC, SIT, and SIC climatology of target moths and predicts the SIC of the next six months. A spatially constrained loss function NIIEE is employed to train the model considering sea ice distribution. We employ a 20-year (2000-2019) testing set to validate the model's performance. The summer season, Jun. to Sep., is the target period. The detrend ACC, BACC, and MAE are metrics. Comparison experiments with Persistence and seasonal predictions of SEAS5 are made to validate our model's performance. In particular, an ablation experiment is carried out to investigate the role of SIT data in optimizing the predictions around the SPB. A generalization experiment with data from the last four years, 2020-2023, is carried out—the seasonal predictions of Sep. SIEs are analyzed. Finally, we discuss the advantages and disadvantages of our model and the typical CNN-based model, U-Net (IceNet-inspired). Given the mentioned efforts, our study draws the following conclusions.

First, our deep learning model, $SICNet_{season,}$ is skillful in predicting the Arctic sea ice seasonally. Compared with the dynamic model SEAS5, $SICNet_{season}$ optimizes the SPB significantly. The detrended ACC of Sep. SIE predicted by $SICNet_{season}$ in May/Apr. is improved by 7.7%/10.61% over the ACC predicted by the SEAS5. Compared with the anomaly persistence benchmark, the mentioned improvement is 41.02%/36.33%. Our deep learning model significantly reduces prediction errors of Sep.'s SIC on seasonal scales compared to SEAS5 and Persistence, a 20-30% reduction measured by MAE.

Second, the spring SIT data is key in optimizing the predictions around the SPB, contributing to a more than 20% ACC enhancement in Sep.'s SIE at four to five months lead predictions. By including SIT data, the MAEs in the Beaufort Sea, the East Siberian Sea, and the Laptev Sea are reduced by more than 10% compared with those without SIT data.

Third, our model achieves good generalization in predicting the Sep. SIEs of 2020-2023. When predicting the Sep.'s SIE in 2020/2023 (second/sixth lowest record) in May, $SICNet_{season}$ achieved a BACC of 82.25%/82.08%, about 12%/10% higher than Persistence and SEAS5.

Fourth, our transformer-based $SICNet_{season}$ is more skillful than the CNN-based U-Net (IceNet-inspired) model in seasonal sea ice predictions. Our $SICNet_{season}$ model optimizes the ACC gap with an improvement of 31.8%/20.8% at May's predictions over the U-Net (IceNet-inspired). The $SICNet_{season}$ exhibits a lower dependency on SIE trends and lower smooth results than the CNN-based model. This is due to the attention mechanism of the transformer operator extracting "personalized" global dependencies, while the CNN operator captures the most "common" local dependencies globally. The "common" local dependencies smooth the map and depend more on the trend than "personalized" ones.

Code and data availability

The code, the exact input/output data, and the saved well-trained weights of the developed model $SICNet_{season}$ are available at https://doi.org/10.5281/zenodo.14561423.

Acknowledgment

This work was supported by the National Science Foundation of China (42206202), Laoshan Laboratory Innovation Project (LSKJ202202302), and the National Science Foundation of China (42221005), in part by the China-Portugal Xinghai "Belt and Road" (2022YFE0204600).

Author contribution

All authors designed the experiments and carried them out. Yibin Ren developed and evaluated the model. Xiaofeng Li designed experiments and revised the manuscript. Yunhe Wang analyzed the experimental results.

Competing interests

The authors declare no competing interests.

References

Andersson, T. R., Hosking, J. S., Pérez-Ortiz, M., Paige, B., Elliott, A., Russell, C., Law, S., Jones, D. C., Wilkinson, J., Phillips, T., Byrne, J., Tietsche, S., Sarojini, B. B., Blanchard-Wrigglesworth, E., Aksenov, Y., Downie, R., and Shuckburgh, E.: Seasonal Arctic sea ice forecasting with probabilistic deep learning, Nat Commun, 12, https://doi.org/10.1038/s41467-021-25257-4, 2021.

Blackport, R., Screen, J. A., van der Wiel, K., and Bintanja, R.: Minimal influence of reduced Arctic sea ice on coincident cold winters in mid-latitudes, Nat Clim Chang, 9, 697–704, https://doi.org/10.1038/s41558-019-0551-4, 2019.

Blanchard-Wrigglesworth, E., Armour, K. C., Bitz, C. M., and Deweaver, E.: Persistence and inherent predictability of arctic sea ice in a GCM ensemble and observations, J Clim, 24, 231–250, https://doi.org/10.1175/2010JCLI3775.1, 2011.

Blanchard-Wrigglesworth, E., Cullather, R. I., Wang, W., Zhang, J., and Bitz, C. M.: Model forecast skill and sensitivity to initial conditions in the seasonal Sea Ice Outlook, Geophys Res Lett, 42, 8042–8048, https://doi.org/10.1002/2015GL065860, 2015.

Blanchard-Wrigglesworth, E., Bushuk, M., Massonnet, F., Hamilton, L. C., Bitz, C. M., Meier, W. N., and Bhatt, U. S.: Forecast Skill of the Arctic Sea Ice Outlook 2008–2022, Geophys Res Lett, 50, https://doi.org/10.1029/2022GL102531, 2023.

Bonan, D. B., Bushuk, M., and Winton, M.: A spring barrier for regional predictions of summer Arctic sea ice, Geophys Res Lett, 46, 5937–5947, https://doi.org/10.1029/2019GL082947, 2019.

Bushuk, M., Ali, S., Bailey, D. A., Bao, Q., Batté, L., Bhatt, U. S., Blanchard-Wrigglesworth, E., Blockley, E., Cawley, G., Chi, J., Counillon, F., Coulombe, P. G., Cullather, R. I., Diebold, F. X., Dirkson, A., Exarchou, E., Göbel, M., Gregory, W., Guemas, V., Hamilton, L., He, B., Horvath, S., Ionita, M., Kay, J. E., Kim, E., Kimura, N., Kondrashov, D., Labe, Z. M., Lee, W. S., Lee, Y. J., Li, C., Li, X., Lin, Y., Liu, Y., Maslowski, W., Massonnet, F., Meier, W. N., Merryfield, W. J., Myint, H., Acosta Navarro, J. C., Petty, A., Qiao, F., Schröder, D., Schweiger, A., Shu, Q., Sigmond, M., Steele, M., Stroeve, J., Sun, N., Tietsche, S., Tsamados, M., Wang, K., Wang, J., Wang, W., Wang, Y., Wang, Y., Williams, J., Yang, Q., Yuan, X., Zhang, J., and Zhang, Y.: Predicting September Arctic Sea Ice: A Multimodel Seasonal Skill Comparison, Bull Am Meteorol Soc, 105, E1170–E1203, https://doi.org/10.1175/BAMS-D-23-0163.1, 2024.

Bushuk, M., Giannakis, D., and Majda, A. J.: Arctic Sea Ice Reemergence: The Role of Large-Scale Oceanic and Atmospheric Variability, J Clim, 28, 5477–5509, https://doi.org/https://doi.org/10.1175/JCLI-D-14-00354.1, 2015.

Bushuk, M., Winton, M., Bonan, D. B., Blanchard-Wrigglesworth, E., and Delworth, T. L.: A mechanism for the Arctic sea ice spring predictability barrier, Geophys Res Lett, 47, https://doi.org/10.1029/2020GL088335, 2020.

Bushuk, M., Zhang, Y., Winton, M., Hurlin, B., Delworth, T., Lu, F., Jia, L., Zhang, L., Cooke, W., Harrison, M., Johnson, N. C., Kapnick, S., Mchugh, C., Murakami, H., Rosati, A., Tseng, K.-C., Wittenberg, A. T., Yang, X., and Zeng, A. F.: Mechanisms of Regional Arctic Sea Ice Predictability in Two Dynamical Seasonal Forecast Systems, https://doi.org/10.1175/JCLI-D-21, n.d.

Cao Hu and Wang, Y. and C. J. and J. D. and Z. X. and T. Q. and W. M.: Swin-Unet: Unet-Like Pure Transformer for Medical Image Segmentation, in: Computer Vision – ECCV 2022 Workshops, 205–218, 2023.

Cao, Y., Liang, S., Chen, X., He, T., Wang, D., and Cheng, X.: Enhanced wintertime greenhouse effect reinforcing Arctic amplification and initial sea-ice melting, Sci Rep, 7, https://doi.org/10.1038/s41598-017-08545-2, 2017.

Cao, Y., Liang, S., Sun, L., Liu, J., Cheng, X., Wang, D., Chen, Y., Yu, M., and Feng, K.: Trans-Arctic shipping routes expanding faster than the model projections, Global Environmental Change, 73, https://doi.org/10.1016/j.gloenvcha.2022.102488, 2022.

DiGirolamo, N. E., Parkinson, C. L., Cavalieri, D. J., Gloersen, P., and Zwally, H. J.: Sea ice concentrations from Nimbus-7 SMMR and DMSP SSM/I-SSMIS passive microwave data., Boulder, Colorado USA. NASA National Snow and Ice Data Center Distributed Active Archive Center, https://doi.org/10.5067/MPYG15WAA4WX, 2022.

Chevallier, M., Mélia, D. S. Y., Voldoire, A., Déqué, M., and Garric, G.: Seasonal forecasts of the pan-arctic sea ice extent using a GCM-based seasonal prediction system, J Clim, 26, 6092–6104, https://doi.org/10.1175/JCLI-D-12-00612.1, 2013.

Cohen, J., Screen, J. A., Furtado, J. C., Barlow, M., Whittleston, D., Coumou, D., Francis, J., Dethloff, K., Entekhabi, D., Overland, J., and Jones, J.: Recent Arctic amplification and extreme mid-latitude weather, https://doi.org/10.1038/ngeo2234, 2014.

Collow, T. W., Wang, W., Kumar, A., and Zhang, J.: Improving arctic sea ice prediction using PIOMAS initial sea ice thickness in a coupled ocean-atmosphere model, Mon Weather Rev, 143, 4618–4630, https://doi.org/10.1175/MWR-D-15-0097.1, 2015.

Day, J. J., Tietsche, S., and Hawkins, E.: Pan-arctic and regional sea ice predictability: Initialization month dependence, J Clim, 27, 4371–4390, https://doi.org/10.1175/JCLI-D-13-00614.1, 2014.

Ding, Q., Schweiger, A., L'Heureux, M., Battisti, D. S., Po-Chedley, S., Johnson, N. C., Blanchard-Wrigglesworth, E., Harnos, K., Zhang, Q., Eastman, R., and Steig, E. J.: Influence of high-latitude atmospheric circulation changes on summertime Arctic sea ice, Nat Clim Chang, 7, 289–295, https://doi.org/10.1038/nclimate3241, 2017.

Dong, X., Yang, Q., Nie, Y., Zampieri, L., Wang, J., Liu, J., and Chen, D.: Antarctic sea ice prediction with A convolutional long short-term memory network, https://doi.org/10.1016/j.ocemod.2024.102386, 1 August 2024.

England, M. R., Eisenman, I., Lutsko, N. J., and Wagner, T. J. W.: The Recent Emergence of Arctic Amplification, Geophys Res Lett, 48, https://doi.org/10.1029/2021GL094086, 2021.

Francis, J. A. and Vavrus, S. J.: Evidence linking Arctic amplification to extreme weather in mid-latitudes, Geophys Res Lett, 39, https://doi.org/10.1029/2012GL051000, 2012.

Goessling, H. F., Tietsche, S., Day, J. J., Hawkins, E., and Jung, T.: Predictability of the Arctic sea ice edge, Geophys Res Lett, 43, 1642–1650, https://doi.org/10.1002/2015GL067232, 2016.

Gregory, W., Tsamados, M., Stroeve, J., and Sollich, P.: Regional september sea ice forecasting with complex networks and gaussian processes, Weather Forecast, 35, 793–806, https://doi.org/10.1175/WAF-D-19-0107.1, 2020.

Guemas, V., Blanchard-Wrigglesworth, E., Chevallier, M., Day, J. J., Déqué, M., Doblas-Reyes, F. J., Fučkar, N. S., Germe, A., Hawkins, E., Keeley, S., Koenigk, T., Salas y Mélia, D., and Tietsche, S.: A review on Arctic sea-ice predictability and prediction on seasonal to decadal time-scales, Quarterly Journal of the Royal Meteorological Society, 142, 546–561, https://doi.org/10.1002/qj.2401, 2016.

Jahn, A., Holland, M. M., and Kay, J. E.: Projections of an ice-free Arctic Ocean, https://doi.org/10.1038/s43017-023-00515-9, 1 March 2024.

Jenkins, M. and Dai, A.: The Impact of Sea-Ice Loss on Arctic Climate Feedbacks and Their Role for Arctic Amplification, Geophys Res Lett, 48, https://doi.org/10.1029/2021GL094599, 2021.

Johnson, S. J., Stockdale, T. N., Ferranti, L., Balmaseda, M. A., Molteni, F., Magnusson, L., Tietsche, S., Decremer, D., Weisheimer, A., Balsamo, G., Keeley, S. P. E., Mogensen, K., Zuo, H., and Monge-Sanz, B. M.: SEAS5: The new ECMWF seasonal forecast system, Geosci Model Dev, 12, 1087–1117, https://doi.org/10.5194/gmd-12-1087-2019, 2019.

Jun Kim, Y., Kim, H. C., Han, D., Lee, S., and Im, J.: Prediction of monthly Arctic sea ice concentrations using satellite and reanalysis data based on convolutional neural networks, Cryosphere, 14, 1083–1104, https://doi.org/10.5194/tc-14-1083-2020, 2020.

Kapsch, M. L., Graversen, R. G., and Tjernström, M.: Springtime atmospheric energy transport and the control of Arctic summer sea-ice extent, Nat Clim Chang, 3, 744–748, https://doi.org/10.1038/nclimate1884, 2013.

Kim, Y. H., Min, S. K., Gillett, N. P., Notz, D., and Malinina, E.: Observationally-constrained projections of an ice-free Arctic even under a low emission scenario, Nat Commun, 14, https://doi.org/10.1038/s41467-023-38511-8, 2023.

Kumar, A., Perlwitz, J., Eischeid, J., Quan, X., Xu, T., Zhang, T., Hoerling, M., Jha, B., and Wang, W.: Contribution of sea ice loss to Arctic amplification, Geophys Res Lett, 37, https://doi.org/10.1029/2010GL045022, 2010.

Kwok, R., Cunningham, G. F., Kacimi, S., Webster, M. A., Kurtz, N. T., and Petty, A. A.: Decay of the Snow Cover Over Arctic Sea Ice From ICESat-2 Acquisitions During Summer Melt in 2019, Geophys Res Lett, 47, https://doi.org/10.1029/2020GL088209, 2020.

Landy, J. C., Dawson, G. J., Tsamados, M., Bushuk, M., Stroeve, J. C., Howell, S. E. L., Krumpen, T., Babb, D. G., Komarov, A. S., Heorton, H. D. B. S., Belter, H. J., and Aksenov, Y.: A year-round satellite sea-ice thickness record from CryoSat-2, Nature, 609, 517–522, https://doi.org/10.1038/s41586-022-05058-5, 2022.

Liang, X., Zhao, F., Li, C., Zhang, L., and Li, B.: Evaluation of ArcIOPS sea ice forecasting products during the ninth chinare-arctic in summer 2018, Adv Polar Sci, 31, 14–25, https://doi.org/10.13679/j.advps.2019.0019, 2020.

Lindsay, R. W., Zhang, J., Schweiger, A. J., and Steele, M. A.: Seasonal predictions of ice extent in the Arctic Ocean, J Geophys Res Oceans, 113, https://doi.org/10.1029/2007JC004259, 2008.

Liu, Z., Risi, C., Codron, F., He, X., Poulsen, C. J., Wei, Z., Chen, D., Li, S., and Bowen, G. J.: Acceleration of western Arctic sea ice loss linked to the Pacific North American pattern, Nat Commun, 12, https://doi.org/10.1038/s41467-021-21830-z, 2021a.

Liu, Z., Lin, Y., Cao, Y., Hu, H., Wei, Y., Zhang, Z., Lin, S., and Guo, B.: Swin Transformer: Hierarchical Vision Transformer using Shifted Windows, in: 2021 IEEE/CVF International Conference on Computer Vision (ICCV), 9992–10002, https://doi.org/10.1109/ICCV48922.2021.00986, 2021b.

Li, X., Liu, B., Zheng, G., Ren, Y., Zhang, S., Liu, Y., Gao, L., Liu, Y., Zhang, B., and Wang, F.: Deep-learning-based information mining from ocean remote-sensing imagery, Natl Sci Rev, 7, https://doi.org/10.1093/NSR/NWAA047, 2021.

Li, Y., Qiu, Y., Jia, G., Yu, S., Zhang, Y., Huang, L., and Lepparanta, M.: An Explainable Deep Learning Model for Daily Sea Ice Concentration Forecast, IEEE Transactions on Geoscience and Remote Sensing, 62, 1–17, https://doi.org/10.1109/TGRS.2024.3386930, 2024.

Merryfield, W. J., Lee, W. S., Wang, W., Chen, M., and Kumar, A.: Multi-system seasonal predictions of Arctic sea ice, Geophys Res Lett, 40, 1551–1556, https://doi.org/10.1002/grl.50317, 2013.

Min, C., Yang, Q., Chen, D., Yang, Y., Zhou, X., Shu, Q., and Liu, J.: The Emerging Arctic Shipping Corridors, Geophys Res Lett, 49, https://doi.org/10.1029/2022GL099157, 2022.

Msadek, R., Vecchi, G. A., Winton, M., and Gudgel, R. G.: Importance of initial conditions in seasonal predictions of Arctic sea ice extent, Geophys Res Lett, 41, 5208–5215, https://doi.org/10.1002/2014GL060799, 2014.

Mu, B., Luo, X., Yuan, S., and Liang, X.: IceTFT v1.0.0: interpretable long-term prediction of Arctic sea ice extent with deep learning, Geosci Model Dev, 16, 4677–4697, https://doi.org/10.5194/gmd-16-4677-2023, 2023.

Mu, L., Nerger, L., Tang, Q., Loza, S. N., Sidorenko, D., Wang, Q., Semmler, T., Zampieri, L., Losch, M., and Goessling, H. F.: Toward a data assimilation system for seamless sea ice prediction based on the AWI climate model, J Adv Model Earth Syst, 12, https://doi.org/10.1029/2019MS001937, 2020.

Nakanowatari, T., Inoue, J., Zhang, J., Watanabe, E., and Kuroda, H.: A New Norm for Seasonal Sea Ice Advance Predictability in the Chukchi Sea: Rising Influence of Ocean Heat Advection, J Clim, 35, 2723–2740, https://doi.org/10.1175/JCLI-D-21-0425.1, 2022.

Olonscheck, D., Mauritsen, T., and Notz, D.: Arctic sea-ice variability is primarily driven by atmospheric temperature fluctuations, Nat Geosci, 12, 430–434, https://doi.org/10.1038/s41561-019-0363-1, 2019.

Palerme, C., Lavergne, T., Rusin, J., Melsom, A., Brajard, J., Kvanum, A. F., MacDonald Sørensen, A., Bertino, L., and Müller, M.: Improving short-term sea ice concentration forecasts using deep learning, Cryosphere, 18, 2161–2176, https://doi.org/10.5194/tc-18-2161-2024, 2024.

Pithan, F. and Mauritsen, T.: Arctic amplification dominated by temperature feedbacks in contemporary climate models, Nat Geosci, 7, 181–184, https://doi.org/10.1038/ngeo2071, 2014.

Reichstein, M., Camps-Valls, G., Stevens, B., Jung, M., Denzler, J., Carvalhais, N., and Prabhat: Deep learning and process understanding for data-driven Earth system science, Nature, 566, 195–204, https://doi.org/10.1038/s41586-019-0912-1, 2019.

Ren, Y. and Li, X.: Predicting the Daily Sea Ice Concentration on a Subseasonal Scale of the Pan-Arctic During the Melting Season by a Deep Learning Model, IEEE Transactions on Geoscience and Remote Sensing, 61, https://doi.org/10.1109/TGRS.2023.3279089, 2023.

Ren, Y., Li, X., and Zhang, W.: A data-driven deep learning model for weekly sea ice concentration prediction of the Pan-Arctic during the melting season, IEEE Transactions on Geoscience and Remote Sensing, 60, https://doi.org/10.1109/TGRS.2022.3177600, 2022.

Schweiger, A., Lindsay, R., Zhang, J., Steele, M., Stern, H., and Kwok, R.: Uncertainty in modeled Arctic sea ice volume, J Geophys Res Oceans, 116, https://doi.org/10.1029/2011JC007084, 2011.

Screen, J. A. and Simmonds, I.: The central role of diminishing sea ice in recent Arctic temperature amplification, Nature, 464, 1334–1337, 2010.

Screen, J. A., Simmonds, I., Deser, C., and Tomas, R.: The atmospheric response to three decades of observed arctic sea ice loss, J Clim, 26, 1230–1248, https://doi.org/10.1175/JCLI-D-12-00063.1, 2013.

Shu, Q., Wang, Q., Arthun, M., Wang, S., Song, Z., Zhang, M., and Qiao, F.: Arctic Ocean Amplification in a warming climate in CMIP6 models, Sci Adv, 8, eabn9755, https://doi.org/10.1126/sciadv.abn9755, 2022.

Sigmond, M., Fyfe, J. C., Flato, G. M., Kharin, V. V., and Merryfield, W. J.: Seasonal forecast skill of Arctic sea ice area in a dynamical forecast system, Geophys Res Lett, 40, 529–534, https://doi.org/10.1002/grl.50129, 2013.

Song, C., Zhu, J., and Li, X.: Assessments of Data-Driven Deep Learning Models on One-Month Predictions of Pan-Arctic Sea Ice Thickness, Adv Atmos Sci, 41, 1379–1390, https://doi.org/10.1007/s00376-023-3259-3, 2024.

Stroeve, J. and Notz, D.: Insights on past and future sea-ice evolution from combining observations and models, Glob Planet Change, 135, 119–132, https://doi.org/https://doi.org/10.1016/j.gloplacha.2015.10.011, 2015.

Tietsche, S., Day, J. J., Guemas, V., Hurlin, W. J., Keeley, S. P. E., Matei, D., Msadek, R., Collins, M., and Hawkins, E.: Seasonal to interannual Arctic sea ice predictability in current global climate models, Geophys Res Lett, 41, 1035–1043, https://doi.org/10.1002/2013GL058755, 2014.

Wang, L., Yuan, X., Ting, M., and Li, C.: Predicting summer arctic sea ice concentration intraseasonal variability using a vector autoregressive model, J Clim, 29, 1529–1543, https://doi.org/10.1175/JCLI-D-15-0313.1, 2016.

Wang, W., Chen, M., and Kumar, A.: Seasonal prediction of arctic sea ice extent from a coupled dynamical forecast system, Mon Weather Rev, 141, 1375–1394, https://doi.org/10.1175/MWR-D-12-00057.1, 2013.

Wang, Y., Yuan, X., Bi, H., Bushuk, M., Liang, Y., Li, C., and Huang, H.: Reassessing seasonal sea ice predictability of the Pacific-Arctic sector using a Markov model, Cryosphere, 16, 1141–1156, https://doi.org/10.5194/tc-16-1141-2022, 2022.

Wu, A., Che, T., Li, X., and Zhu, X.: Routeview: an intelligent route planning system for ships sailing through Arctic ice zones based on big Earth data, Int J Digit Earth, 15, 1588–1613, https://doi.org/10.1080/17538947.2022.2126016, 2022.

Yang, Q., Mu, L., Wu, X., Liu, J., Zheng, F., Zhang, J., and Li, C.: Improving Arctic sea ice seasonal outlook by ensemble prediction using an ice-ocean model, Atmos Res, 227, 14–23, https://doi.org/10.1016/j.atmosres.2019.04.021, 2019.

Yang, Z., Liu, J., Song, M., Hu, Y., Yang, Q., and Fan, K.: Extended seasonal prediction of Antarctic sea ice using ANTSIC-UNet, EGUsphere, 2024, 1–25, https://doi.org/10.5194/egusphere-2024-1001, 2024.

Yuan, X., Chen, D., Li, C., Wang, L., and Wang, W.: Arctic sea ice seasonal prediction by a linear markov model, J Clim, 29, 8151–8173, https://doi.org/10.1175/JCLI-D-15-0858.s1, 2016.

Zampieri, L., Goessling, H. F., and Jung, T.: Bright Prospects for Arctic Sea Ice Prediction on Subseasonal Time Scales, Geophys Res Lett, 45, 9731–9738, https://doi.org/10.1029/2018GL079394, 2018.

Zeng, J., Yang, Q., Li, X., Yuan, X., Bushuk, M., and Chen, D.: Reducing the Spring Barrier in Predicting Summer Arctic Sea Ice Concentration, Geophys Res Lett, 50, https://doi.org/10.1029/2022GL102115, 2023.

Zhang, J. and Rothrock, D. A.: Modeling Global Sea Ice with a Thickness and Enthalpy Distribution Model in Generalized Curvilinear Coordinates, Mon Weather Rev, 131, 845–861, https://doi.org/https://doi.org/10.1175/1520-0493(2003)131<0845:MGSIWA>2.0.CO;2, 2003.

Zhang, J., Steele, M., Lindsay, R., Schweiger, A., and Morison, J.: Ensemble 1-Year predictions of Arctic sea ice for the spring and summer of 2008, Geophys Res Lett, 35, https://doi.org/10.1029/2008GL033244, 2008.

Zhang, Y.-F., Bushuk, M., Winton, M., Hurlin, B., Delworth, T., Harrison, M., Jia, L., Lu, F., Rosati, A., and Yang, X.: Subseasonal-to-Seasonal Arctic Sea Ice Forecast Skill Improvement from Sea Ice Concentration Assimilation, J Clim, 35, 4233–4252, https://doi.org/https://doi.org/10.1175/JCLI-D-21-0548.1, 2022.

Zhang, Y. F., Bushuk, M., Winton, M., Hurlin, B., Gregory, W., Landy, J., and Jia, L.: Improvements in September Arctic Sea Ice Predictions Via Assimilation of Summer CryoSat-2 Sea Ice Thickness Observations, Geophys Res Lett, 50, https://doi.org/10.1029/2023GL105672, 2023.

Zhu, Y., Qin, M., Dai, P., Wu, S., Fu, Z., Chen, Z., Zhang, L., Wang, Y., and Du, Z.: Deep Learning-Based Seasonal Forecast of Sea Ice Considering Atmospheric Conditions, Journal of Geophysical Research: Atmospheres, 128, https://doi.org/10.1029/2023JD039521, 2023.